Role and recruitment of the TagL peptidoglycan-binding protein during Type VI secretion system biogenesis

Yoann G Santin, Claire Camy, Abdelrahim Zoued, Thierry Doan, Marie-Stéphanie Aschtgen, E. Cascales

Role and recruitment of the TagL peptidoglycan-binding protein during Type VI secretion system biogenesis

Yoann G. SANTIN, Claire E. CAMY, Abdelrahim ZOUED[†], Thierry DOAN, Marie-Stéphanie ASCHTGEN[§], and Eric CASCALES*

Running title: TagL functional analysis

Laboratoire d'Ingénierie des Systèmes Macromoléculaires (LISM), Institut de Microbiologie de la Méditerranée (IMM), Aix-Marseille Université - CNRS, UMR 7255, 31 chemin Joseph Aiguier CS7071, 13402 Marseille Cedex 09, France

[†] Current address: Howard Hughes Medical Institute, Brigham and Women's Hospital, Division of Infectious Diseases and Harvard Medical School, Department of Microbiology and Immunobiology, Boston, Massachusetts, USA.

[§] Current address: Department of Microbiology, Tumor and Cell Biology, Karolinska Institutet, 171 77 Stockholm, Sweden.

* To whom correspondence should be addressed:
Eric Cascales (cascales@imm.cnrs.fr)

Abstract

The Type VI secretion system (T6SS) is an injection apparatus that uses a spring-like mechanism for effector delivery. The contractile tail is composed of a needle tipped by a sharpened spike and wrapped by the sheath that polymerizes in an extended conformation on the assembly platform or baseplate. Contraction of the sheath propels the needle and effectors associated with it into target cells. The passage of the needle through the cell envelope of the attacker is assured by a dedicated trans-envelope channel complex. This membrane complex (MC) comprises the TssJ lipoprotein, and the TssL and TssM inner membrane proteins. MC assembly is a hierarchized mechanism in which the different subunits are recruited in a specific order: TssJ, TssM and then TssL. Once assembled, the MC serves as a docking station for the baseplate. In enteroaggregative *Escherichia coli*, the MC is accessorized by TagL, a peptidoglycan-binding (PGB) inner membrane-anchored protein. Here we show that the PGB domain is the only functional domain of TagL, and that the N-terminal transmembrane region mediates contact with the TssL transmembrane helix. Finally, we conduct fluorescence microscopy experiments to position TagL in the T6SS biogenesis pathway, demonstrating that TagL is recruited to the membrane complex downstream TssL and is not required for baseplate docking.

Keywords

Protein transport; membrane complex; peptidoglycan; assembly pathway, domain swapping.

Importance

Bacteria use weapons to deliver effector into target cells. One of these weapons, called Type VI secretion system (T6SS), could be compared to a nano-speargun using a spring-like mechanism for effector injection. By targeting bacteria and eukaryotic cells, the T6SS reshapes bacterial communities and hijacks host cell defences. In enteroaggregative *Escherichia coli*, the T6SS is a multiprotein machine that comprises a cytoplasmic tail and a peptidoglycan-anchored trans-envelope channel. In this work, we show that TagL comprises a N-terminal domain that mediates contact with the channel, and a peptidoglycan-binding domain that binds the cell wall. We then determine at which stage of T6SS biogenesis TagL is recruited and how TagL absence impacts the assembly pathway.

Introduction

Bacteria have evolved sophisticated mechanisms to attack or defend against competitors that share the same environment, such as different bacterial species, amoeba, other unicellular microorganisms, or fungi (1,2). Among those, the Type VI secretion system (T6SS) is a multi-protein complex that is widespread in Gram-negative bacteria (3-9). The T6SS is capable of delivering effectors in bacteria and eukaryotic cells and is therefore an important player in inter-bacterial competition and pathogenesis (10-14). At the molecular level, the T6SS can be architecturally and mechanistically compared to a nano-crossbow or -speargun (6,15). It is related to a broad family of contractile injection systems (CIS) that include bacteriophages, R-pyocins and anti-feeding prophages (16-19). CIS comprise a spring-like structure, called the tail, composed of an inner tube terminated by a spike, wrapped by a contractile sheath and built on an assembly platform (18,19). Once in contact with the target cell, the sheath contracts and hence propels the inner tube/spike needle. The T6SS tail tube is made of Hcp hexamers stacked on each other and tipped by a trimer of the VgrG spike protein, which is further sharpened by the metal-bound PAAR protein (20-24). The contractile sheath that wraps the inner tube is composed of two proteins, TssB and TssC (15,25-28). The T6SS tail assembly platform or baseplate comprises the TssEFGK subunits that form a complex similar to bacteriophage baseplate wedges (29-32). Similarly to bacteriophages, six TssEFGK wedges polymerize around the VgrG spike to form the functional baseplate (31-32). Once the baseplate is assembled, the TssA protein will control the polymerization of the tube and of the sheath by adding tube and sheath building blocks from the distal end until it contacts the TagA stopper at the opposite membrane (33-37). In addition to the conserved CIS tail, T6SSs comprise an additional trans-envelope complex that anchors the tail to the cell envelope, positions the tail for firing toward the exterior, and serves

as a channel for the passage of the inner tube (38,39). The membrane complex (MC) is composed of three proteins: TssJ, TssL and TssM. TssJ is an outer membrane lipoprotein whereas TssL and TssM are two inner membrane proteins, inserted by one and three transmembrane helices (TMHs) respectively (40-43). TssL dimerizes and interacts with TssM by its single TMH (42,44,45), whereas the C-terminal region of the TssM periplasmic domain binds to TssJ (39,46). The negative-stain and cryo-electron microscopy, and cryo-electron tomography structures of the 1.7-MDa T6SS MC from enteroaggregative *Escherichia coli* (EAEC) have been reported, defining a rocket-like shape, with a large cytoplasmic base followed by arches likely corresponding to the TssL and TssM TMHs, and by pillars crossing the periplasm and corresponding to the TssM periplasmic domain and TssJ lipoprotein (39,47,48). The central portion of the MC defines a channel that is narrowed at the periplasmic entrance and closed at its outer membrane extremity, suggesting that the MC undergoes significant conformational changes during firing to allow the passage of the needle (39,47). The cytoplasmic base of the membrane complex represents the docking station for the assembled baseplate, mainly by contacts between the C-terminal domain of the baseplate TssK subunit with the cytoplasmic domains of TssL and TssM (30,32,43,49-52). The assembly of the membrane complex starts with the positioning of the TssJ lipoprotein and the ordered recruitment of TssM and TssL (39). Polymerization of the TssJLM complex to assemble the MC requires local remodeling of the peptidoglycan, which is assured by a dedicated or housekeeping transglycosylase (53,54). In most T6SS, the MC is stably anchored to the cell wall by a peptidoglycan-binding (PGB) domain (38,55). In most cases, the PGB domain is fused to the C-terminus of the TssL TMH (Fig. 1). However, other T6SS have evolved different strategies to be anchored to the peptidoglycan layer, such as accessory inner membrane or periplasmic proteins bearing a PGB domain (55). In EAEC, the PGB domain is carried by the accessory protein TagL that associates with the membrane complex by directly

111 interacting with TssL (38). TagL is constituted of three TMHs and the periplasmic PGB
112 domain (Fig. 1)(38). Mutations within the PGB that prevent peptidoglycan binding *in vivo*
113 and *in vitro* abolish T6SS activity, demonstrating that TagL-mediated anchoring to the cell
114 wall is necessary for T6SS function (38). Here we show that fusing the TagL PGB to the C-
115 terminus of TssL is sufficient to compensate for the absence of *tagL*, demonstrating that the
116 PGB domain is the only functional domain of TagL. We further demonstrate that TagL-TssL
117 complex formation is mediated by interactions between their TMHs. We then generated a
118 functional sfGFP-TagL protein and showed by fluorescence microscopy that it co-localizes
119 with TssL at the base of the sheath, and is recruited downstream TssL but upstream baseplate
120 docking. Finally, microscopy recordings of functional GFP fusions to T6SS subunits in
121 absence of *tagL* demonstrate that TagL is not necessary for recruitment of TssA and of the
122 baseplate, but required for sheath polymerization.
123
124 **Results**
125 **TagL PGB fusion to TssL bypasses the requirements for full-length TagL.**
126 The EAEC T6SS *sci1* gene cluster encodes TagL, a three-TMH inner membrane
127 protein that bears a periplasmic peptidoglycan-binding (PGB) domain (38) (Fig. 1). Binding
128 to the cell wall is required for T6SS function as TagL PGB amino-acid substitutions that
129 prevent *in vitro* and *in vivo* interaction with the peptidoglycan abolish T6SS activity (38).
130 However, although TagL is not broadly conserved in T6SSs, T6SS gene clusters usually
131 encode a PGB domain that can be either carried by an accessory protein or fused to the TssL
132 core component (55) (Fig. 1). We therefore asked whether the N-terminal transmembrane
133 portion of TagL is necessary for T6SS function. For this, we engineered a strain deleted of
134 both *tssL* and *tagL*. Δ*tssL-tagL* cells, as well as Δ*tssL-tagL* cells expressing *tssL* or *tagL* only,
135 were unable to release Hcp in the culture supernatant, and to outcompete *E. coli* K-12 cells in

antibacterial assays (Fig. 2A and Fig. 2B), in agreement with the essential roles of TssL and TagL in EAEC T6SS (38,42). However, a plasmid-borne fragment encoding both TssL and TagL complemented the phenotypes associated with the Δ*tssL-tagL* deletion to wild-type levels (Fig. 2A and Fig. 2B). Interestingly, fusion of the TagL periplasmic PGB domain at the C-terminus of TssL to yield the TssL-PGB chimera protein was sufficient to promote T6SS activity in Δ*tssL-tagL* cells (Fig. 2A and Fig. 2B). This result demonstrates that the C-terminal PGB domain is the only functional domain of TagL. In agreement with this observation, production of the TssL-PGB chimera protein bearing substitutions that prevent anchorage of the PGB domain to the cell wall (TssL-PGB*, N494L/L497N/S498A/R501Q/A502D substitutions; 38) was unable to restore T6SS activity in Δ*tssL-tagL* cells (Fig. 2A and Fig. 2B).

The TagL N-terminal region mediates interaction with the TssL TMH.

The observation that the PGB domain of TagL (orange in Fig. 3A and 3B) is necessary and sufficient for T6SS raised the question of the role of its N-terminal region, that comprises three TMHs, a short periplasmic linker connecting TMH1 and TMH2, and a cytoplasmic domain located between TMH2 and TMH3 (blue in Fig. 3A and 3B). We hypothesized that this region might engage in the interaction with TssL. To test whether the TagL N-terminal region is important for TagL-TssL complex formation, we performed co-precipitation analyses. As previously shown (38), precipitation of 6×His-tagged TagL on nickel magnetic beads co-precipitated TssL (Fig. 3C, lanes 3 and 4). However, TagL did not co-precipitate $TssL_C$, a TssL variant deleted of its C-terminal TMH (red in Fig. 3A and 3B)(Fig. 3C, lanes 5 and 6), suggesting that TagL-TssL complex formation does not require interactions between their cytoplasmic domain, and thus that it likely involves their TMHs. In agreement with this hypothesis, a TagL variant deleted of its periplasmic domain but retaining its three TMHs ($TagL\Delta_P$, blue in Fig. 3A and 3B) co-precipitated TssL at comparable levels to full-length

TagL (Fig. 3C, lanes 7 and 8). From these results, we conclude that the TagL periplasmic region, that includes the PGB domain, and the TssL cytoplasmic domain, do not contribute to TagL-TssL complex formation and hence that the interaction between the two partners is likely mediated by their TMHs. Taken together, the results of Figures 2 and 3 suggest that the TagL PGB domain is a functional module for T6SS activity whereas its TMHs are required for recruitment to the T6SS MC via direct interactions with the TssL TMH.

TagL colocalizes with the membrane complex at the base of the tail.

To define the localization and dynamics of TagL in wild-type EAEC cells, we engineered a chromosomally-encoded superfolder Green Fluorescent Protein (sfGFP) fusion to TagL, by inserting the sfGFP-encoding fragment in frame, downstream the *tagL* ATG start codon. Hence, sfGFP-TagL is produced from the native locus, under the expression signals of *tagL*. Antibacterial assays demonstrated that this sfGFP-TagL fusion is functional as sfGFP-TagL-producing cells outcompete *E. coli* K-12 competitor cells (Fig. S1). Fluorescence microscopy analyses showed that sfGFP-TagL clusters in foci in EAEC cells (Fig. 4A). Time-lapse recordings further showed that these foci remain static (Fig. 4A). Quantitative and distribution analyses demonstrated that most cells contain less than 2 foci per cell (Fig. 4B), and that sfGFP-TagL foci localize in all the cell body with an underrepresentation at the cell poles (Fig. 4C). The number of foci per cell and their spatial distribution is comparable to what has been previously reported for sfGFP-TssL and sfGFP-TssM in EAEC (39). In agreement with this observation, and with previous protein-protein interaction data showing that TagL interacts with TssL (38; Fig. 3C), fluorescence microscopy analyses of EAEC cells producing both sfGFP-TagL and TssL fused to mCherry (mCh-TssL) demonstrated that in most cases TagL and TssL co-localize (Fig. 4D). In some cases, only a mCh-TssL focus was visible without evidence for the presence of sfGFP-TagL (see white arrow in Fig. 4D). While

we cannot rule out that some MC may assemble without TagL, we hypothesize that these cases represent assembly intermediates, in which TagL has not been recruited yet to the MC. Nevertheless, these results suggest that TagL co-localizes with the MC, and hence should be located at the base of the extended sheath. Indeed, sfGFP-TagL foci localize at one extremity of the T6SS sheath (Fig. 4E). Time-lapse recordings further showed that the sheaths contract on sfGFP-TagL foci (Fig. 4F) demonstrating that TagL localizes at the base of the sheath.

Recruitment and role of TagL during T6SS biogenesis in EAEC

T6SS biogenesis is a hierarchized pathway, in which subunits or complexes are recruited in a strict order. T6SS biogenesis is initiated by the assembly of the MC (39) and pursued by the docking of the BP (30,32) and the extension of the tail tube/sheath structure (30,39). TssA is recruited to the TssJM complex and helps the recruitment of the BP complex prior to tail tube/sheath polymerization (33). Finally, TagA stops tail tube/sheath polymerization, and maintains the sheath under the extended conformation (37). We therefore wished to determine at which step TagL is recruited and how TagL absence impacts the T6SS biogenesis pathway.

To define the requirements for TagL recruitment at the T6SS, we fused sfGFP to TagL in various mutant backgrounds deleted of T6SS genes. Fig. 5A shows that sfGFP-TagL localizes in foci in absence of TssK, TssA or of the TssBC sheath subunits. In addition, statistical analyses showed that the absence of these T6SS subunits does not significantly impact the localization and distribution of sfGFP-TagL foci (Fig. S2). These results suggest that TagL is recruited to the apparatus prior to BP assembly and docking to the MC. Biogenesis of the MC starts with the positioning of TssJ and the subsequent recruitment of TssM and TssL (39). Then, TssJLM complexes polymerize to assemble the MC once the cell wall has been locally degraded by MltE (54). Fluorescence microscopy experiments showed

that TssJ, TssM, TssL and MltE are necessary for sfGFP-TagL recruitment (Fig. 5A), suggesting that TagL binds to the MC once this complex has been fully assembled.

Based on these results, we hypothesized that TagL should not be required for MC assembly, but will be necessary for BP docking. To verify this hypothesis, we deleted the *tagL* gene in EAEC cells producing sfGFP-TssM, -TssL, -TssA, TssK-sfGFP or TssB-mCh from their native loci. As expected, the absence of TagL does not impact the recruitment of TssM nor TssL (Fig. 5B). However, by contrast to our initial hypothesis, TssA and TssK formed foci in absence of TagL (Fig. 5B). Statistical analyses showed that the number of sfGFP-TssM, -TssL, -TssA, and TssK-sfGFP foci per cell is not impacted by the absence of TagL (Fig. S3), suggesting that TagL does not participate to the stability of the T6SS MC and BP complexes. Taken together, these results demonstrate that TagL binding to the MC is not a prerequisite for BP docking. Interestingly, although the absence of TagL does not prevent TssA recruitment to the MC, TssA forms static foci which do not move to the opposite membrane in Δ*tagL* cells (Fig. S4A) suggesting that TagL is necessary for sheath extension. Indeed, no sheath structure was observable in absence of TagL (Fig. 5B). Finally, because previous data have shown that the MC is static over time (39), we asked whether TagL-mediated interaction with the cell wall stabilizes the MC and prevents its diffusion in the cell envelope. This hypothesis is however unlikely as time-lapse recordings showed that sfGFP-TssM foci remain static in absence of TagL (Fig. S4B).

Taken together our fluorescence microscopy observations demonstrate that TagL is recruited once the MC is fully assembled, is dispensable for the assembly of the MC and for the docking of the BP, but is necessary for tail sheath extension (Fig. 5C).

Discussion

In this work, we provide details on the role of the TagL peptidoglycan-binding protein for T6SS function, and during T6SS biogenesis in EAEC.

TagL comprises two domains: a N-terminal domain constituted of three TMHs that mediate interaction with the TssL TMH, and a C-terminal domain that binds the cell wall. Our results show that the PGB domain is the only functional domain of TagL, as a fusion protein between TssL and the TagL PGB domain is sufficient to support T6SS activity. Based on this observation, we hypothesize that the TagL N-terminal transmembrane domain is only necessary to bind TssL and hence to accessorize the T6SS with the PGB domain. Interestingly, previous analyses have shown that most T6SS gene clusters encode for proteins with peptidoglycan-binding motifs. However, these proteins come in many flavors: inner membrane-anchored accessory proteins such as TagL or TagP, predicted periplasmic proteins such as TagN or TagW, or PGB domain fused to the TssL core-component ("specialized" TssL) (55). A detailed phylogenetic study of these proteins would be required to understand how these genes have been acquired, how they have evolved to accessorize the T6SS. One interesting question is whether specialized TssL arose from a reduction of the gene cluster by fusing the PGB domain of TagL/TagN/TagP/TagW to TssL, or whether TagL/TagN/TagP/TagW evolved from the partition of the TssL core and PGB domains. Our observations that TagL PGB domain fusion to TssL bypasses the requirement for full-length TagL and that its TMHs are only necessary to mediate contact with TssL tend to support the reduction hypothesis.

By using deletion variants, we have shown that TssL-TagL complex formation is mediated by their TMHs. While we have not defined which of the three TagL TMHs is implicated in the interaction with the TssL C-terminal TMH, previous studies have reported that the TssL TMH is engaged in interaction with itself and with the TssM TMHs (39,43,45). Because there is no conserved sequence homology or helical motifs between the TagL and

TssM TMHs, we suggest that TagL and TssM do not share the same face of interaction on the TssL TMHs, and hence that TssL-TagL and TssL-TssM interactions are not exclusive. This hypothesis is in agreement with previous data reporting the co-precipitation of a ternary TssM-TssL-TagL complex (38). These observations suggest that in addition to the tryptophan residues engaged in π-π interactions in the TssL TMH dimer (45), two additional faces of the TssL TMH are involved in TssM and TagL interactions. Further studies need to be performed to better understand the organization of the TMHs of the TssM-TssL-TagL complex in the inner membrane.

In this work, we performed a comprehensive fluorescence microscopy analysis to position TagL in the T6SS biogenesis pathway. By using a functional sfGFP-TagL fusion, we showed that TagL co-localizes with TssL at the base of the extended sheath, in agreement with TagL association with the MC. From our time-lapse fluorescence recordings of cells producing both sfGFP-TagL and TssB-mCherry, one can notice that TagL remains at the MC during sheath contraction, suggesting that TagL is associated with TssL during all the T6SS mechanism of action. We can hypothesize that TagL-mediated PG-anchoring is important to stabilize the MC and to prevent its dissociation by the mechanical strength generated by sheath contraction (15). Our analyses of sfGFP-TagL foci formation in various T6SS mutant backgrounds revealed that positioning TagL at the site of T6SS assembly requires TssJ, TssM, TssL and MltE, but does not require TssK, TssA or TssBC. Therefore TagL is recruited to the MC prior to BP docking. Because the MltE lytic transglycosylase enables full assembly of the MC by locally remodeling the cell wall (54), these results suggest that TagL is recruited to the MC when its assembly is completed (Fig. 5C). Indeed, TagL, and TagL-mediated PG-anchoring, is not required for MC assembly, in agreement with the facts that TagL is an accessory protein that is not conserved in all T6SS (38,55) and that the MC can be purified from *E. coli* K-12 cells lacking TagL (39). However, although TagL is recruited

upstream the BP, it is not necessary for BP docking to the MC (Fig. 5C). This result clearly shows that the T6SS biogenesis pathway is not a strict linear pathway, with the ordered recruitment of one subunit after the other, but rather that independent branches exist. However, while the BP docks to the MC in Δ*tagL* cells, extension of the tail/tube cannot proceed in absence of TagL. This observation hence suggests that once the BP docks to the MC, TagL mediates a structural modification of the MC or BP that is required to initiate sheath extension. Electron microscopy models of the MC bound to TagL or of the MC-BP complex would likely provide further information on the impact of TagL on the conformations of the MC or BP.

Material and Methods

Bacterial strains, media, growth conditions, and chemicals.

Bacteria strains are listed in Supplemental Table S1. *Escherichia coli* K-12 DH5α and W3110 strains were used for cloning procedures, and co-immunoprecipitations, respectively. *Escherichia coli* K-12 W3110 cells carrying the pFPV-mCherry plasmid (mCherry under the constitutive and strong ribosomal *rpsM* promoter, Amp^R; 56) were used as recipients for the antibacterial competition assays. The enteroaggregative *E. coli* (EAEC) wild-type strain 17-2, its Δ*tagL*, Δ*tssM*, Δ*tssL*, Δ*tssJ*, Δ*tssA*, and Δ*tssK* derivatives and 17-2 strains producing the TssB-mCh, TssB-sfGFP, sfGFP-TssA, sfGFP-TssM, sfGFP-TssL, mCh-TssL, and TssK-sfGFP fusion from their native chromosomal loci have been previously described (30,33,38-40,49). Strains were routinely grown in LB broth at 37°C with aeration. For induction of the T6SS *sci1* genes, strains were grown in Sci1 inducing medium (SIM; M9 minimal medium supplemented with glycerol 0.25%, vitamin B1 1 $\mu g.mL^{-1}$, casaminoacids 40 $\mu g.mL^{-1}$, and 10% v/v of LB; 57). Plasmids and mutations were maintained by the addition of ampicillin (100 $\mu g.mL^{-1}$ for K-12, 200 $\mu g.mL^{-1}$ for EAEC), kanamycin (50 $\mu g.mL^{-1}$ for K-12, 50 $\mu g.mL^{-1}$ for chromosomal insertion on EAEC, 100 $\mu g.mL^{-1}$ for plasmid-bearing EAEC). Gene

312 expression from pASK-IBA vectors was induced for 30 min with 0.05 µg.mL^{-1} of anhydrotetracyclin
313 (AHT, IBA Technologies).
314
315 **Strain construction.**
316 The 17-2 derivative strains were engineered by λ-red recombination (58) using plasmid pKOBEG
317 (59). For construction of the 17-2 strain deleted of *tagL* or of both *tssL* and *tagL* (Δ*tssL-tagL*), a
318 kanamycin cassette was amplified from plasmid pKD4 (58) with primers carrying 50-bp extensions
319 corresponding to the 5' and 3' sequences of the region to be deleted. For construction of 17-2 strain
320 derivatives producing sfGFP-TagL, a kanamycine-sfGFP cassette was amplified from the pKD4-Nter-
321 sfGFP vector (39) with primers carrying 50-bp extensions corresponding to the upstream and
322 downstream regions of the *tagL* initiation codon. PCR products were electroporated into target cells,
323 and λ-red-mediated recombination at the proper locus was verified by PCR. The excision of the
324 kanamycin cassette, when possible, was then obtained by production of the Flp recombinase using
325 pCP20 (58). The final strains were verified by PCR.
326
327 **Plasmid construction.**
328 Plasmids used in this study are listed in Supplemental Table S1. Polymerase Chain Reactions (PCR)
329 were performed with a Biometra thermocycler, using the Pfu Turbo DNA polymerase (Stratagene).
330 Custom oligonucleotides were synthesized by Sigma-Aldrich and are listed in Supplemental Table S1.
331 The pASK-IBA37(+) vector producing N-terminally 6×His-tagged TagL (initially called pIBA-28;
332 38), the FLAG-tagged TssL or TssL fused to the periplasmic domain (amino-acids 360-576) of TagL
333 (TssL-PGB, initially named pIBA-SciP and pIBA-SciP-PG; 42), and the pOK12 derivatives producing
334 N-terminally HA-tagged Hcp (38) or TssL (initially named pOK-SciP-HA; 38) have been previously
335 described. The pOK12 plasmid producing the TssL cytoplasmic domain (amino-acids 1-186, $TssL_C$)
336 was constructed by standard restriction/ligation cloning by inserting a *Eco*RI-*tssL$_C$*-*Xho*I fragment into
337 EcoRI-XhoI-digested pOK12 derivative plasmid pMS600 (40). Plasmid producing TagL deleted of
338 the periplasmic region (TagLΔ$_P$) has been constructed by replacing *tagL* codon 366 by a TAA stop
339 codon on pIBA-TagL, using site-directed mutagenesis and primers carrying the desired substitutions.

The pIBA-TssL-TagL plasmid, producing both TssL and TagL, and pIBA-TssL-PGB*, producing TssL fused to the TagL mutated PGB domain (PGB*, Asn494Leu-Leu497Asn-Ser498Ala-Arg501Gln-Ala502Asp substitutions; 38), have been constructed by restriction-free cloning (38,60). Briefly, the sequences encoding the TssL protein, or the mutated PGB domain of TagL were amplified from 17-2 DNA and plasmid pIBA-TagL-PG* (38) respectively, with oligonucleotides carrying 5' extensions annealing upstream and downstream the site of insertion on the target plasmid. The products of the first PCR were then used as oligonucleotides for a second PCR using the target vector as template. The *tssL* fragment was inserted into plasmid pIBA-TagL, whereas the PGB*-encoding fragment was inserted into plasmid pIBA-TssL. All constructs have been verified by restriction analyses and DNA sequencing (Eurofins genomics).

T6SS function reporter assays.

The Hcp release assay was performed as described (40), using plasmid pOK-Hcp_{HA}, except that cells were grown in SIM to an absorbance at λ = 600 nm (A_{600}) of 0.6. The periplasmic TolB protein was used as control for cell integrity. The interbacterial competition assay has been performed as described (61) with modifications as follows: (i) *E. coli* W3110 cells constitutively expressing the mCherry from plasmid pFPV-mCherry (Amp^R; 56) has been used as recipients, (ii) fluorescence measurements with the TECAN microplate reader were performed by exciting the mCherry at λ = 575 nm, and recording its emission at λ = 610 nm, and (iii) survival of recipient cells was calculated by counting colony forming units (cfu) on recipient-selective LB plates supplemented with ampicillin.

Co-precipitation on nickel magnetic beads.

5×10^9 *E. coli* W3110 cells producing the proteins of interest were harvested, and resuspended in CelLytic B lysis reagent (Sigma-Aldrich) supplemented with 100 $\mu g.mL^{-1}$ lysozyme, 100 $\mu g.mL^{-1}$ DNase, protease inhibitors (Complete, Roche), and 1.65 mM octylphenoxy poly(ethyleneoxy)ethanol (Igepal® CA-630, Sigma-Aldrich). After 30-min incubation at 25°C with strong agitation, unsolubilized material was discarded by centrifugation for 20 min at 20,000×*g*. The cleared lysates were supplemented with imidazole 10 mM and incubated with Nickel magnetic beads

(PureProteome™, Millipore) for 2 hours at room temperature on a wheel. Magnetic beads were then washed three times with CelLytic B lysis reagent supplemented with Igepal CA-630 and imidazole 20 mM, resuspended in non-reducing Laemmli loading dye, and subjected to sodium-dodecylsulphate poly-acrylamide gel electrophoresis (SDS-PAGE) and immuno-blot analyses using monoclonal anti-His and anti-HA antibodies.

Fluorescence microscopy and data analysis.

Cells producing the chromosomal sfGFP or mCherry fusion proteins were grown in SIM to a A_{600} of 0.6–0.8, harvested and resuspended in SIM to a A_{600} of 8. Cells were then spotted on a thin pad of SIM supplemented with 2% agarose, covered with a cover slip and incubated for 20-30 min at room temperature before microscopy acquisition. Fluorescence microscopy recordings were performed with a Nikon Eclipse Ti microscope equipped with an Orcaflash 4.0 LT digital camera (Hamamatsu) and a perfect focus system (PFS) to automatically maintain focus so that the point of interest within a specimen is always kept in sharp focus at all times despite mechanical or thermal perturbations. All fluorescence images were acquired with a minimal exposure time to minimize bleaching and phototoxicity effects. Exposure times were typically 30 ms for phase contrast, 250 ms for sfGFP fusion proteins, and 200 ms for TssB-mCh and TssL-mCh. The images shown in the figures are representative regions cropped from large fields, from at least triplicate experiments. Images were analyzed using ImageJ (62) and the MicrobeJ plugin (63). Statistical dataset analysis was performed using the R software environment (https://www.r-project.org/).

Miscellaneous.

SDS-PAGE and transfer onto nitrocellulose membranes (Amersham Protran 0.2 µm, GE Healthcare) have been performed with standard procedures using Mini-Protean II systems (Biorad). After protein transfer, membranes were probed with primary antibodies and goat secondary antibodies coupled to alkaline phosphatase. Immunodetections were performed in alkaline buffer in presence of 5-bromo-4-chloro-3-indolylphosphate and nitroblue tetrazolium. The anti-FLAG (clone M2, Sigma-Aldrich),

anti-HA (clone HA-7, Sigma-Aldrich) anti-Histidine tag (clone AD1.1.10, Biorad) monoclonal antibodies, and alkaline phosphatase-conjugated goat anti-mouse and anti-rabbit secondary antibodies (Beckman Coulter) are commercially available. The anti-TolB polyclonal antibodies are from the laboratory collection.

Acknowledgments

We thank Leon Espinosa for helpful discussions and advices on fluorescence microscopy, Laure Journet, Dukas Jurėnas and Yassine Cherrak for critical reading of the manuscript, laboratory members for discussions, Moly Ba, Isabelle Bringer, Annick Brun and Oliver Uderso, for technical assistance, and Jean-Phil Monce-Lipp for encouragements. This work was supported by the Centre National de la Recherche Scientifique (CNRS), the Aix-Marseille Université (AMU), and grants from the Agence Nationale de la Recherche (ANR-10-JCJC-1303, ANR-14-CE14-0006 and ANR-17-CE11-0039) and Fondation pour la Recherche Médicale (FRM, DEQ20180339165) to EC. YGS, AZ and MSA were supported by doctoral fellowships from the French Ministère de l'Education Supérieure et de la Recherche. The end-of-thesis of MSA was supported by an Attaché Temporaire d'Enseignement et de Recherche (ATER) fellowship from the Aix-Marseille Université. The end-of-thesis of AZ was supported by a fellowship from the FRM (FDT20140931060). The funders had no role in study design, data collection and interpretation, or the decision to submit the work for publication.

References

1. Chassaing B, Cascales E. 2018. Antibacterial weapons: targeted destruction in the microbiota. Trends Microbiol 26:329–338.

2. Coyne MJ, Comstock LE. 2019. Type VI secretion systems and the gut microbiota. Microbiol Spectr 7:2.

3. Bingle LE, Bailey CM, Pallen MJ. 2008. Type VI secretion: a beginner's guide. Curr Opin Microbiol 11:3–8.

4. Cascales E. 2008. The type VI secretion toolkit. EMBO Rep 9:735–741.

5. Boyer F, Fichant G, Berthod J, Vandenbrouck Y, Attree I. 2009. Dissecting the bacterial type VI secretion system by a genome wide in silico analysis: what can be learned from available microbial genomic resources? BMC Genomics 10:104.

6. Zoued A, Brunet YR, Durand E, Aschtgen MS, Logger L, Douzi B, Journet L, Cambillau C, Cascales E. 2014. Architecture and assembly of the type VI secretion system. Biochim Biophys Acta 1843:1664–1673.

7. Ho BT, Dong TG, Mekalanos JJ. 2014. A view to a kill: the bacterial type VI secretion system. Cell Host Microbe 15:9–21.

8. Cianfanelli FR, Monlezun L, Coulthurst SJ. 2016. Aim, load, fire: the type VI secretion system, a bacterial nanoweapon. Trends Microbiol 24:51–62.

9. Basler M. 2015. Type VI secretion system: secretion by a contractile nanomachine. Philos Trans R Soc Lond B Biol Sci 370:20150021.

10. Russell AB, Peterson SB, Mougous JD. 2014. Type VI secretion system effectors: poisons with a purpose. Nat Rev Microbiol 12:137–148.

11. Durand E, Cambillau C, Cascales E, Journet L. 2014. VgrG, Tae, Tle, and beyond: the versatile arsenal of type VI secretion effectors. Trends Microbiol 22:498–507.

12. Alcoforado Diniz J, Liu YC, Coulthurst SJ. 2015. Molecular weaponry: diverse effectors delivered by the Type VI secretion system. Cell Microbiol 17:1742–1751.

13. Hachani A, Wood TE, Filloux A. 2016. Type VI secretion and anti-host effectors. Curr Opin Microbiol 29:81–93.

14. Trunk K, Peltier J, Liu YC, Dill BD, Walker L, Gow NAR, Stark MJR, Quinn J, Strahl H, Trost M, Coulthurst SJ. 2018. The type VI secretion system deploys antifungal effectors against microbial competitors. Nat Microbiol 3:920–931.

15. Brackmann M, Nazarov S, Wang J, Basler M. 2017. Using force to punch holes: mechanics of contractile nanomachines. Trends Cell Biol 27:623–632.

16. Bönemann G, Pietrosiuk A, Mogk A. 2010. Tubules and donuts: a type VI secretion story. Mol Microbiol 76:815–821.

17. Sarris PF, Ladoukakis ED, Panopoulos NJ, Scoulica EV. 2014. A phage tail-derived element with wide distribution among both prokaryotic domains: a comparative genomic and phylogenetic study. Genome Biol Evol 6:1739–1747.

18. Cascales E. 2017. Microbiology: and *Amoebophilus* invented the machine gun! Curr Biol 27:R1170–R1173.

19. Taylor NMI, van Raaij MJ, Leiman PG. 2018. Contractile injection systems of bacteriophages and related systems. Mol Microbiol 108:6–15.

20. Ballister ER, Lai AH, Zuckermann RN, Cheng Y, Mougous JD. 2008. *In vitro* self-assembly of tailorable nanotubes from a simple protein building block. Proc Natl Acad Sci U S A 105:3733–3738.

21. Leiman PG, Basler M, Ramagopal UA, Bonanno JB, Sauder JM, Pukatzki S, Burley SK, Almo SC, Mekalanos JJ. 2009. Type VI secretion apparatus and phage tail-associated protein complexes share a common evolutionary origin. Proc Natl Acad Sci U S A 106:4154–4159.

22. Shneider MM, Buth SA, Ho BT, Basler M, Mekalanos JJ, Leiman PG. 2013. PAAR-repeat proteins sharpen and diversify the type VI secretion system spike. Nature 500:350–353.

23. Brunet YR, Hénin J, Celia H, Cascales E. 2014. Type VI secretion and bacteriophage tail tubes share a common assembly pathway. EMBO Rep 15:315–321.

24. Renault MG, Zamarreno Beas J, Douzi B, Chabalier M, Zoued A, Brunet YR, Cambillau C, Journet L, Cascales E. 2018. The gp27-like hub of VgrG serves as adaptor to promote Hcp tube assembly. J Mol Biol 430:3143–3156.

25. Basler M, Pilhofer M, Henderson GP, Jensen GJ, Mekalanos JJ. 2012. Type VI secretion requires a dynamic contractile phage tail-like structure. Nature 483:182–186.

26. Kudryashev M, Wang RY, Brackmann M, Scherer S, Maier T, Baker D, DiMaio F, Stahlberg H, Egelman EH, Basler M. 2015. Structure of the type VI secretion system contractile sheath. Cell 160:952–962.

27. Wang J, Brackmann M, Castaño-Díez D, Kudryashev M, Goldie KN, Maier T, Stahlberg H, Basler M. 2017. Cryo-EM structure of the extended type VI secretion system sheath-tube complex. Nat Microbiol 2:1507–1512.

28. Salih O, He S, Planamente S, Stach L, MacDonald JT, Manoli E, Scheres SHW, Filloux A, Freemont PS. 2018. Atomic structure of type VI contractile sheath from *Pseudomonas aeruginosa*. Structure 26:329–336.

29. English G, Byron O, Cianfanelli FR, Prescott AR, Coulthurst SJ. 2014. Biochemical analysis of TssK, a core component of the bacterial type VI secretion system, reveals distinct oligomeric states of TssK and identifies a TssK-TssFG subcomplex. Biochem J 461:291–304.

30. Brunet YR, Zoued A, Boyer F, Douzi B, Cascales E. 2015. The type VI secretion TssEFGK-VgrG phage-like baseplate is recruited to the TssJLM membrane complex *via* multiple contacts and serves as assembly platform for tail tube/sheath polymerization. PLoS Genet 11:e1005545.

31. Nazarov S, Schneider JP, Brackmann M, Goldie KN, Stahlberg H, Basler M. 2018. Cryo-EM reconstruction of Type VI secretion system baseplate and sheath distal end. EMBO J 37: e97103.

32. Cherrak Y, Rapisarda C, Pellarin R, Bouvier G, Bardiaux B, Allain F, Malosse C, Rey M, Chamot-Rooke J, Cascales E, Fronzes R, Durand E. 2018. Biogenesis and structure of a type VI secretion baseplate. Nat Microbiol 3:1404–1416.

33. Zoued A, Durand E, Brunet YR, Spinelli S, Douzi B, Guzzo M, Flaugnatti N, Legrand P, Journet L, Fronzes R, Mignot T, Cambillau C, Cascales E. 2016. Priming and polymerization of a bacterial contractile tail structure. Nature 531:59–63.

34. Zoued A, Durand E, Santin YG, Journet L, Roussel A, Cambillau C, Cascales E. 2017. TssA: The cap protein of the Type VI secretion system tail. Bioessays 39:10.

35. Vettiger A, Winter J, Lin L, Basler M. 2017. The type VI secretion system sheath assembles at the end distal from the membrane anchor. Nat Commun 8:16088.

36. Dix SR, Owen HJ, Sun R, Ahmad A, Shastri S, Spiewak HL, Mosby DJ, Harris MJ, Batters SL, Brooker TA, Tzokov SB, Sedelnikova SE, Baker PJ, Bullough PA, Rice DW, Thomas MS. 2018. Structural insights into the function of type VI secretion system TssA subunits. Nat Commun 9:4765.

37. Santin YG, Doan T, Lebrun R, Espinosa L, Journet L, Cascales E. 2018. *In vivo* TssA proximity labelling during type VI secretion biogenesis reveals TagA as a protein that stops and holds the sheath. Nat Microbiol 3:1304–1313.

38. Aschtgen MS, Gavioli M, Dessen A, Lloubès R, Cascales E. 2010. The SciZ protein anchors the enteroaggregative Escherichia coli Type VI secretion system to the cell wall. Mol Microbiol 75:886–899.

510 39. Durand E, Nguyen VS, Zoued A, Logger L, Péhau-Arnaudet G, Aschtgen MS, Spinelli S,
511 Desmyter A, Bardiaux B, Dujeancourt A, Roussel A, Cambillau C, Cascales E, Fronzes R. 2015.
512 Biogenesis and structure of a type VI secretion membrane core complex. Nature 523:555–560.

513 40. Aschtgen MS, Bernard CS, de Bentzmann S, Lloubès R, Cascales E. 2008. SciN is an outer
514 membrane lipoprotein required for type VI secretion in enteroaggregative *Escherichia coli*. J
515 Bacteriol 190:7523–7531.

516 41. Ma LS, Lin JS, Lai EM. 2009. An IcmF family protein, $ImpL_M$, is an integral inner membrane
517 protein interacting with $_{ImpKL}$, and its walker a motif is required for type VI secretion system-
518 mediated Hcp secretion in *Agrobacterium tumefaciens*. J Bacteriol 191:4316–4329.

519 42. Aschtgen MS, Zoued A, Lloubès R, Journet L, Cascales E. 2012. The C-tail anchored TssL
520 subunit, an essential protein of the enteroaggregative *Escherichia coli* Sci-1 type VI secretion
521 system, is inserted by YidC. Microbiologyopen 1:71–82.

522 43. Logger L, Aschtgen MS, Guérin M, Cascales E, Durand E. 2016. Molecular dissection of the
523 interface between the type VI secretion TssM cytoplasmic domain and the TssG baseplate
524 component. J Mol Biol 428:4424–4437.

525 44. Durand E, Zoued A, Spinelli S, Watson PJ, Aschtgen MS, Journet L, Cambillau C, Cascales E.
526 2012. Structural characterization and oligomerization of the TssL protein, a component shared by
527 bacterial type VI and type IVb secretion systems. J Biol Chem 287:14157–14168.

528 45. Zoued A, Duneau JP, Durand E, España AP, Journet L, Guerlesquin F, Cascales E. 2018.
529 Tryptophan-mediated dimerization of the TssL transmembrane anchor is required for type VI
530 secretion system activity. J Mol Biol 430:987–1003.

531 46. Felisberto-Rodrigues C, Durand E, Aschtgen MS, Blangy S, Ortiz-Lombardia M, Douzi B,
532 Cambillau C, Cascales E. 2011. Towards a structural comprehension of bacterial type VI
533 secretion systems: characterization of the TssJ-TssM complex of an *Escherichia coli* pathovar.
534 PLoS Pathog 7:e1002386.

535 47. Rapisarda C, Cherrak Y, Kooger R, Schmidt V, Pellarin R, Logger L, Cascales E, Pilhofer M,
536 Durand E, Fronzes R. 2019. *In situ* and high-resolution cryo-EM structure of the type VI
537 secretion membrane complex. EMBO J *in press* doi:10.15252/embj.2018100886.

538 48. Yin M, Yan Z, Li X. 2019. Architecture of type VI secretion system membrane core complex.
539 Cell Res 29:251–253.

540 49. Zoued A, Durand E, Bebeacua C, Brunet YR, Douzi B, Cambillau C, Cascales E, Journet L.
541 2013. TssK is a trimeric cytoplasmic protein interacting with components of both phage-like and
542 membrane anchoring complexes of the type VI secretion system. J Biol Chem 288:27031–27041.

543 50. Gerc AJ, Diepold A, Trunk K, Porter M, Rickman C, Armitage JP, Stanley-Wall NR, Coulthurst
544 SJ. 2015. Visualization of the *Serratia* type VI secretion system reveals unprovoked attacks and
545 dynamic assembly. Cell Rep 12:2131–2142.

546 51. Zoued A, Cassaro CJ, Durand E, Douzi B, España AP, Cambillau C, Journet L, Cascales E. 2016.
547 Structure-function analysis of the TssL cytoplasmic domain reveals a new interaction between the
548 type VI secretion baseplate and membrane complexes. J Mol Biol 428:4413–4423.

549 52. Nguyen VS, Logger L, Spinelli S, Legrand P, Huyen Pham TT, Nhung Trinh TT, Cherrak Y,
550 Zoued A, Desmyter A, Durand E, Roussel A, Kellenberger C, Cascales E, Cambillau C. 2017.
551 Type VI secretion TssK baseplate protein exhibits structural similarity with phage receptor-
552 binding proteins and evolved to bind the membrane complex. Nat Microbiol 2:17103.

553 53. Weber BS, Hennon SW, Wright MS, Scott NE, de Berardinis V, Foster LJ, Ayala JA, Adams
554 MD, Feldman MF. 2016. Genetic dissection of the type VI secretion system in *Acinetobacter* and
555 identification of a novel peptidoglycan hydrolase, TagX, required for its biogenesis. MBio.
556 7:e01253-16.

557 54. Santin YG, Cascales E. 2017. Domestication of a housekeeping transglycosylase for assembly of
558 a Type VI secretion system. EMBO Rep 18:138–149.

559 55. Aschtgen MS, Thomas MS, Cascales E. 2010. Anchoring the type VI secretion system to the
560 peptidoglycan: TssL, TagL, TagP... what else? Virulence 1:535–540.

561 56. Drecktrah D, Levine-Wilkinson S, Dam T, Winfree S, Knodler LA, Schroer TA, Steele-Mortimer
562 O. 2008. Dynamic behavior of Salmonella-induced membrane tubules in epithelial cells. Traffic
563 9:2117–2129.

564 57. Brunet YR, Bernard CS, Gavioli M, Lloubès R, Cascales E. 2011. An epigenetic switch involving
565 overlapping Fur and DNA methylation optimizes expression of a type VI secretion gene cluster.
566 PLoS Genet 7:e1002205.

567 58. Datsenko KA, Wanner BL. 2000. One-step inactivation of chromosomal genes in *Escherichia*
568 *coli* K-12 using PCR products. Proc Natl Acad Sci U S A 97:6640–6645.

569 59. Chaveroche MK, Ghigo JM, d'Enfert C. 2000. A rapid method for efficient gene replacement in
570 the filamentous fungus *Aspergillus nidulans*. Nucleic Acids Res 28:E97.

571 60. van den Ent F, Löwe J. 2006. RF cloning: a restriction-free method for inserting target genes into
572 plasmids. J Biochem Biophys Methods 67:67–74.

573 61. Flaugnatti N, Le TT, Canaan S, Aschtgen MS, Nguyen VS, Blangy S, Kellenberger C, Roussel A,
574 Cambillau C, Cascales E, Journet L. 2016. A phospholipase A1 antibacterial type VI secretion
575 effector interacts directly with the C-terminal domain of the VgrG spike protein for delivery. Mol
576 Microbiol 99:1099–1118.

577 62. Schneider CA, Rasband WS, Eliceiri KW. 2012. NIH image to ImageJ: 25 years of image
578 analysis. Nat Methods 9:671–675.

579 63. Ducret A, Quardokus EM, Brun YV. 2016. MicrobeJ, a tool for high throughput bacterial cell
580 detection and quantitative analysis. Nat Microbiol 1:16077.

581

582 **Legend to Figures**

583

584 **Figure 1. Schematic representations of selected T6SS subunits that bind the cell wall.** In
585 EAEC and other species, T6SS gene clusters encode TssL and TagL, a three-TMH protein
586 with a periplasmic peptidoglycan-binding (PGB) domain (shown in orange). In the vast
587 majority of cases, the PGB domain is fused to TssL to yield the TssL-PGB specialized TssL
588 protein. Additional cases have been described by (55). IM, inner membrane; PG,
589 peptidoglycan; OM, outer membrane.

590

591 **Figure 2. The PGB domain is the only functional domain of TagL.** T6SS functional assays
592 of wild-type (WT) cells, and Δ*tssL-tagL* cells bearing the pASK-IBA37(+) empty vector (-) or
593 the pASK-IBA37(+) vector encoding TssL, TagL, both TssL and TagL, the TagL PGB fused
594 to TssL (TssL-PGB) or the mutated TagL PGB fused to TssL (TssL-PGB*). (A) Hcp release
595 was assessed by separating whole cells (C) and supernatant (Sn) fractions from the indicated
596 strains producing HA-tagged Hcp from the pOK-Hcp_{HA} vector. 2×10^8 cells and the TCA-
597 precipitated material of the supernatant from 5×10^8 cells were subjected to 12.5%-acrylamide
598 SDS-PAGE and immunodetected using the anti-HA monoclonal antibody (lower panel) and
599 the anti-TolB polyclonal antibodies (lysis control; upper panel). The positions of Hcp_{HA} and
600 TolB are indicated on the right. Molecular weight markers (in kDa) are indicated on the left.
601 (B) *E. coli* K-12 recipient cells (W3110 mCherry, Amp^R) were mixed with the indicated
602 attacker cells, spotted onto SIM agar plates and incubated for 4 h at 37 °C. The image of a
603 representative bacterial spot is shown below the graph reporting the fluorescence level of the
604 spots (in arbitrary units). The average fluorescence and standard deviation are indicated, as
605 well as the values from nine independent measurements (grey dots). The lower graph reports
606 the number of surviving *E. coli* recipient cells [counted on selective ampicillin medium; in

607 log^{10} of colony-forming units (cfu)]. The grey dots correspond to the nine values from three
608 independent biological replicates. The average is indicated by the horizontal bar.
609
610 **Figure 3. TssL and TagL interact via their TMHs.** (A) Schematic representation of the
611 EAEC T6SS. The membrane complex comprises TssJ (dark grey), TssM (light grey), TssL
612 (red, N-terminal cytoplasmic domain [$TssL_C$]; green, C-terminal TMH) and TagL (blue, N-
613 terminal membrane domain [$TagL\Delta_P$]; orange, C-terminal peptidoglycan-binding domain).
614 The baseplate is shown in green. The contractile tail in shown in blue. The TssA protein,
615 located at the distal end of the tail is shown in red. IM, inner membrane; PG, peptidoglycan;
616 OM, outer membrane. (B) Schematic representation of EAEC TssL and TagL highlighting
617 their topologies (38,42) and different domains (same colours as Fig. 3A). The three TagL
618 TMHs are numbered (1 to 3 from the N-terminus). (C) Co-precipitation assay. Igepal® CA-
619 630-solubilized extracts of *E. coli* cells producing the indicated proteins or protein variants
620 were mixed with Nickel magnetic beads to precipitate 6×His-tagged TagL and interacting
621 partners. The total lysates (T) and eluted (E) material were subjected to 12.5%-acrylamide
622 SDS-PAGE and immunodetected with anti-His (TagL, upper panel) and anti-HA (TssL, lower
623 panel) monoclonal antibodies. The positions of TssL, TagL and their variants are indicated on
624 the right. Molecular weight markers (in kDa) are indicated on the left.
625
626 **Figure 4. Localization, dynamics, and distribution of TagL.** (A) Representative
627 fluorescence microscopy time-lapse recording of wild-type EAEC cells producing sfGFP-
628 TagL. Individual images were taken every 30 s. The white arrowhead highlights the position
629 of one sfGFP-TagL focus showing that it is static over time. Scale bar, 2 μm. (B) Percentage
630 of cells with 0, 1, 2 or >2 sfGFP-TagL foci (n = 1110 cells from four biological replicates).
631 The mean number of foci per cell is 0.67 ± 0.86. (C) Spatial distribution of sfGFP-TagL foci.

Shown is a projection of the foci from *n* = 743 cells on a single cell (from blue to yellow, see heatmap color chart on left). (D) and (E) Representative cells producing sfGFP-TagL and mCherry-TssL (D) or TssB-mCherry (E). From left to right are shown the phase (Phase), sfGFP, and mCherry channels, an overlay of the sfGFP and mCherry channels (merge) and a schematic representation. White and blue arrowheads in panel (D) indicate isolated TssL foci and TssL/TagL foci, respectively. Scale bar, 1 μm. (F) Representative fluorescence microscopy time-lapse recording of a wild-type EAEC cell producing sfGFP-TagL and TssB-mCherry. Individual images were taken every 30 s. A schematic representation is shown below. Scale bar, 1 μm.

Figure 5. Localization and distribution of TagL. (A) Representative fluorescence microscopy fields of WT, Δ*tssJ*, Δ*tssM*, Δ*tssL*, Δ*mltE*, Δ*tssK*, Δ*tssA* and Δ*tssBC* cells producing sfGFP-TagL. Statistical analyses are shown in Fig. S2. Scale bar, 2 μm. (B) Representative fluorescence microscopy fields of wild-type (WT, upper panels) or Δ*tagL* (lower panels) cells producing sfGFP-TssM, sfGFP-TssL, sfGFP-TssA, TssK-sfGFP or TssB-mCh. Statistical analyses are shown in Fig. S3. Scale bar, 1 μm. (C) Schematic representation of the EAEC T6SS biogenesis pathway based on previous studies (30,32,33,39,54) highlighting the position of TagL (shown in green). TagL is recruited after completion of the MC and prior to BP docking (plain green line). TssA recruitment, baseplate positioning (represented by TssK subunit in this study), and tail tube/sheath polymerization (represented by TssBC in this study) are not required for TagL localization, but TagL is necessary for tail tube/sheath polymerization (dotted green line).

Legend to Supplemental Figures

Figure S1. sfGFP-TagL is functional. *E. coli* K-12 recipient cells (W3110 mCherry, Amp^R) were mixed with the indicated attacker cells, spotted onto SIM agar plates and incubated for 4 h at 37 °C. The image of a representative bacterial spot is shown below the graph reporting the fluorescence level of the spots (in arbitrary units). The average fluorescence and standard deviation are indicated, as well as the values from nine independent measurements (grey dots). The lower graph reports the number of surviving *E. coli* recipient cells [counted on selective ampicillin medium; in log^{10} of colony-forming units (cfu)]. The grey dots correspond to the nine values from three independent biological replicates. The average is indicated by the horizontal bar.

Figure S2. Impact of T6SS subunits on TagL localization. Number of sfGFP-TagL foci per cell in Δ*tssJ* (A), Δ*tssM* (B), Δ*tssL* (C), Δ*mltE* (D), Δ*tssK* (E), Δ*tssA* (F), and Δ*tssBC* (G) cells. The number of analyzed cells (*n*) from representative fields of three biological replicates is indicated on top of each graph.

Figure S3. Impact of TagL on T6SS subunits localization. Number of sfGFP-TssM (A), sfGFP-TssL (B), TssK-sfGFP (C), and sfGFP-TssA (D) foci per cell in wild-type (upper graphs) and Δ*tagL* (lower graphs) cells. The number of analyzed cells (*n*) from representative fields of three biological replicates is indicated on top of each graph.

Figure S4. Impact of TagL on TssA and TssM recruitment and dynamics. Representative fluorescence microscopy time-lapse recordings of wild-type (WT, upper panels) or Δ*tagL* (lower panels) cells producing sfGFP-TssA (A) or sfGFP-TssM (B).

680 Individual images were taken every 30 s. White arrowheads indicate the localization and
681 dynamics of a TssA focus. Scale bar is 1 μm.
682

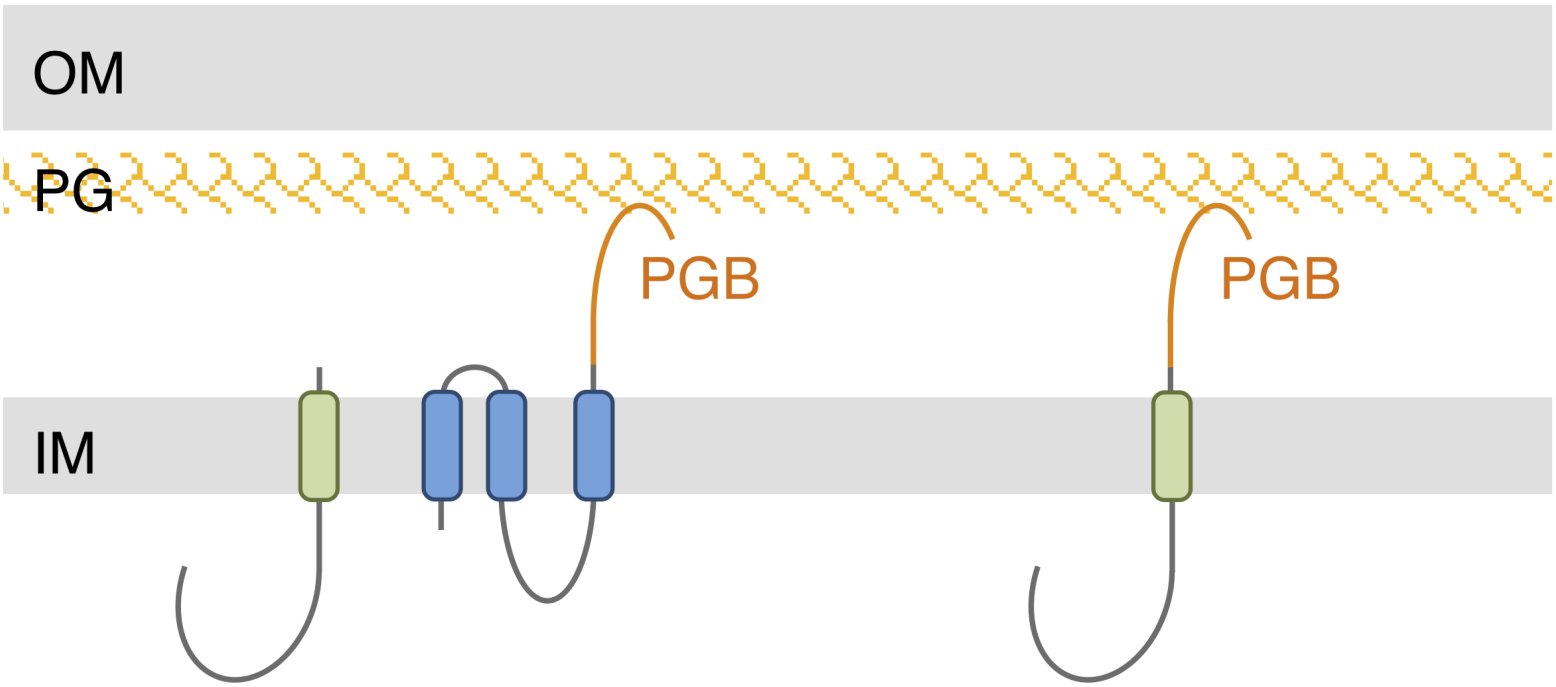

EAEC
Klebsiella pneumoniae
Yersinia pestis

Salmonella enterica
Pseudomonas aeruginosa H1-T6SS
Agrobacterium tumefaciens

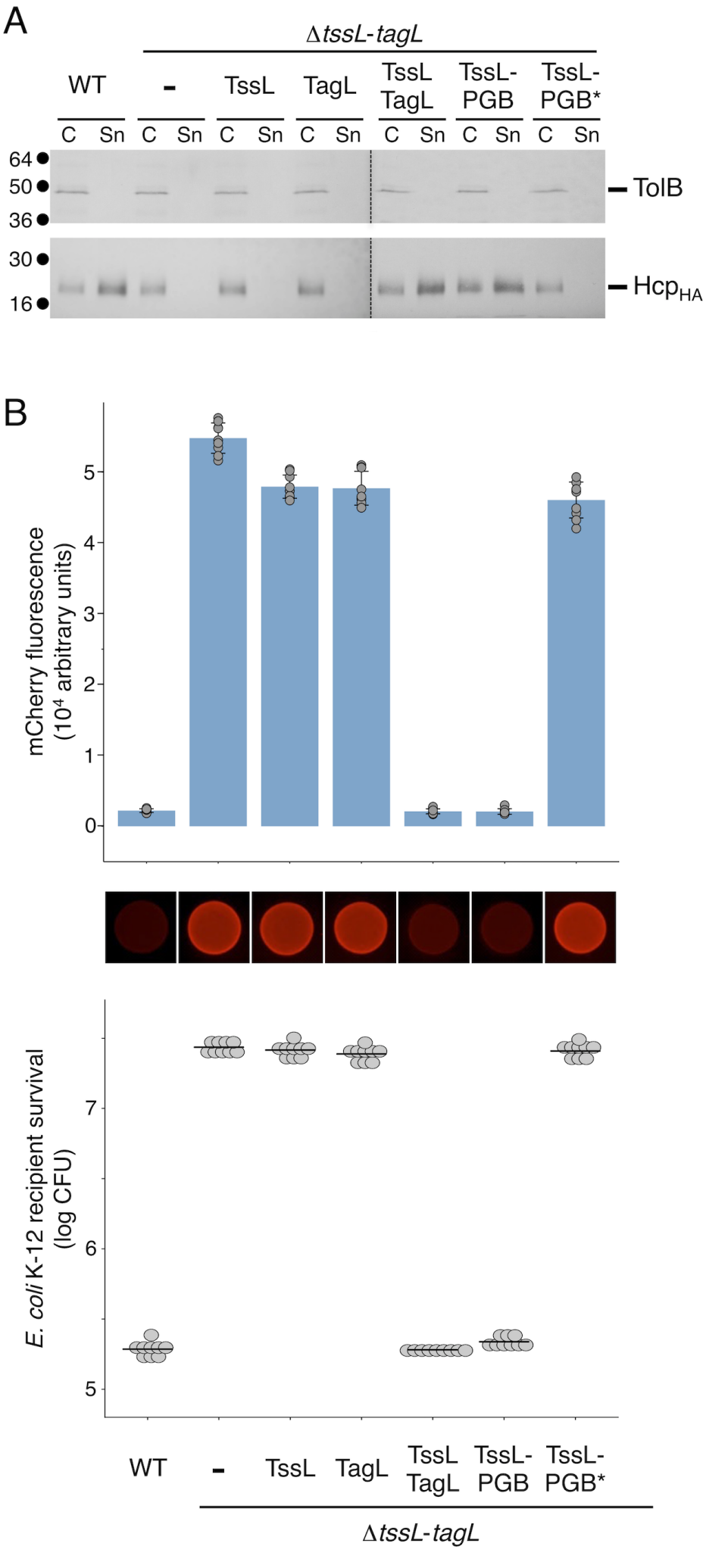
A
ΔtssL-tagL
WT
-
TssL
TagL
TssL TagL
TssL-PGB
TssL-PGB*
C Sn C Sn C Sn C Sn C Sn C Sn C Sn
64
50
36
30
16
TolB
Hcp$_{HA}$
B
mCherry fluorescence (10^4 arbitrary units)
0
1
2
3
4
5
E. coli K-12 recipient survival (log CFU)
5
6
7
WT
-
TssL
TagL
TssL TagL
TssL-PGB
TssL-PGB*
ΔtssL-tagL

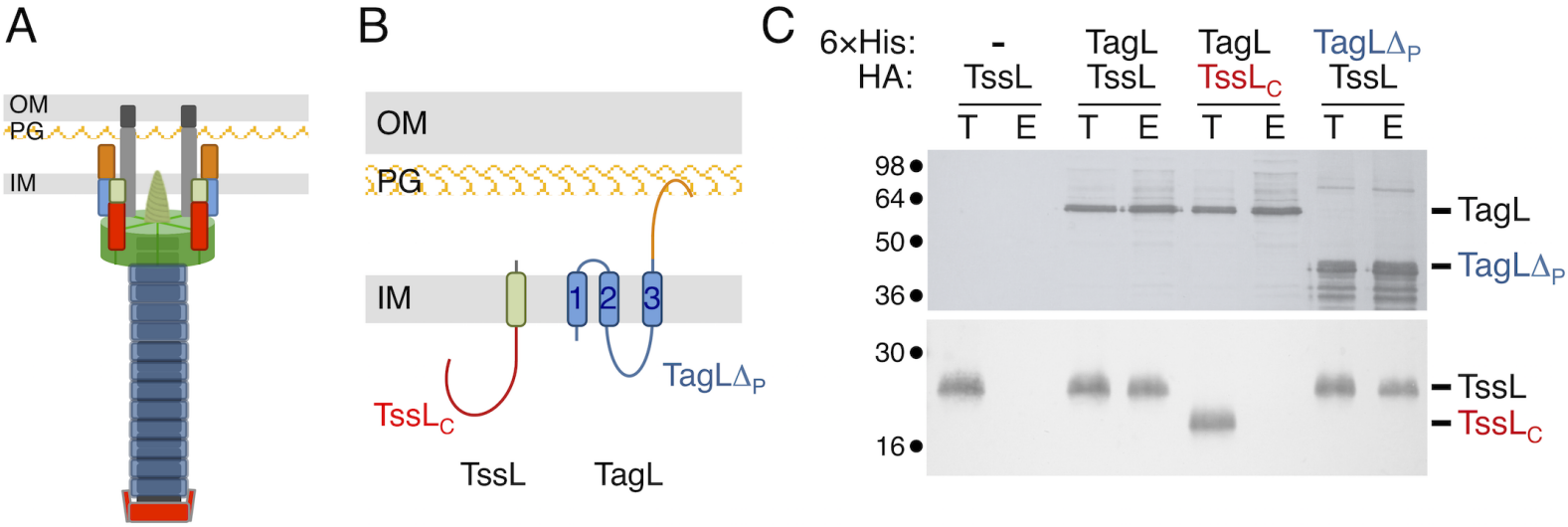
A
OM
PG
IM
B
OM
PG
IM
1
2
3
TagLΔP
TssLC
TssL
TagL
C
6×His:
HA:
-
TssL
TagL
TssL
TagL
TssLC
TagLΔP
TssL
T E T E T E T E
98
64
50
36
30
16
TagL
TagLΔP
TssL
TssLC

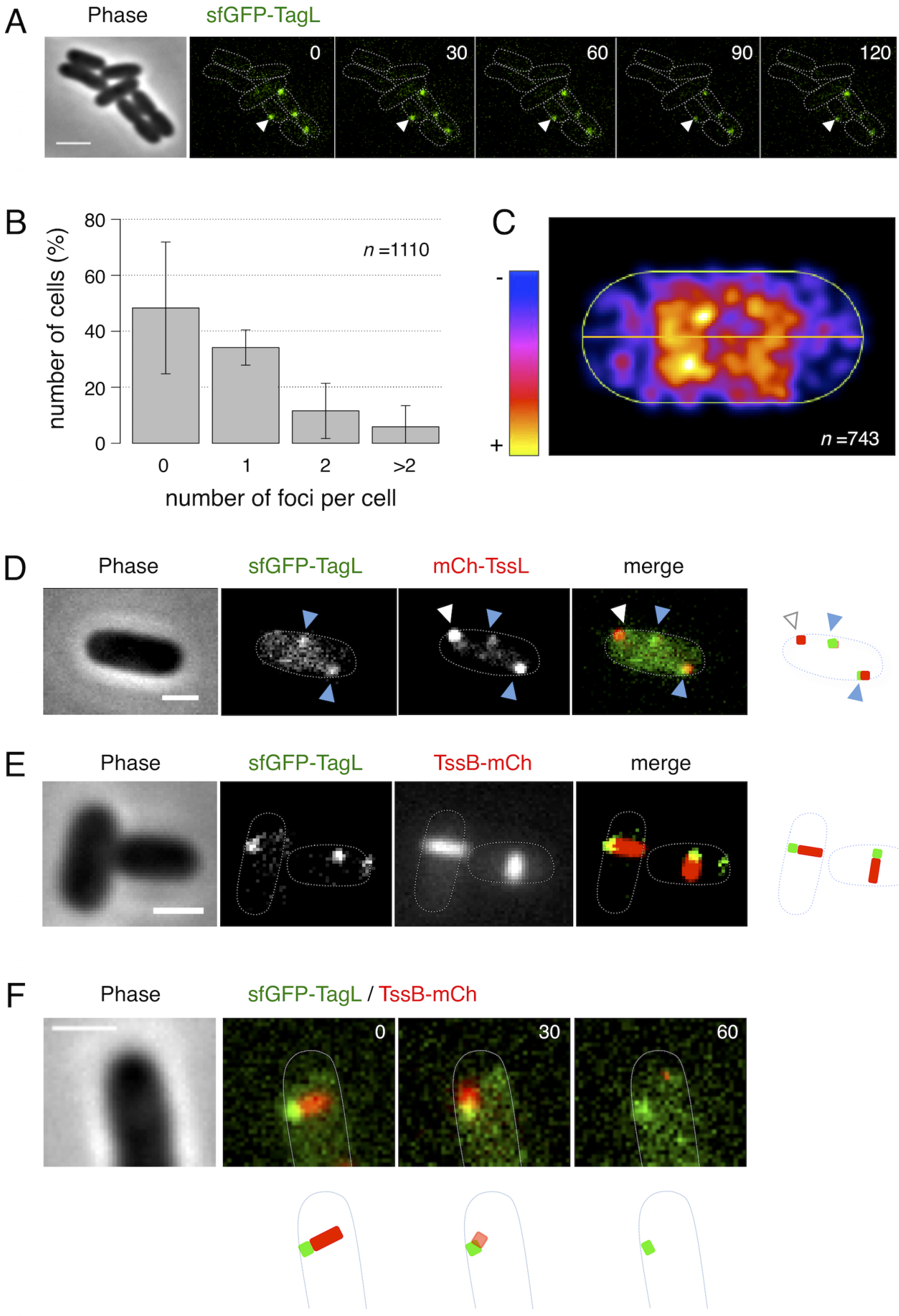
A
Phase
sfGFP-TagL
0
30
60
90
120
B
number of cells (%)
80
60
40
20
0
n =1110
0
1
2
>2
number of foci per cell
C
-
+
n =743
D
Phase
sfGFP-TagL
mCh-TssL
merge
E
Phase
sfGFP-TagL
TssB-mCh
merge
F
Phase
sfGFP-TagL / TssB-mCh
0
30
60

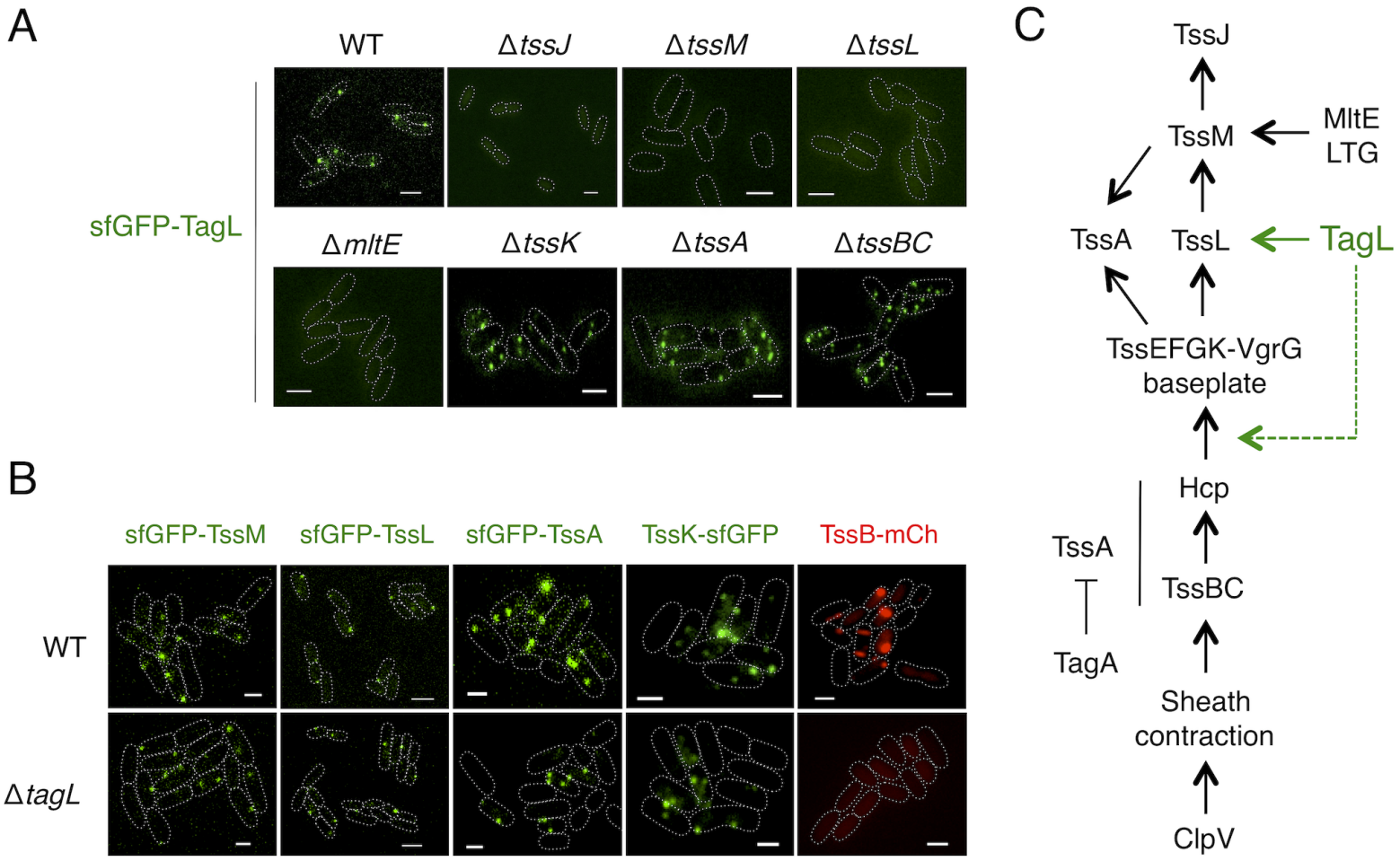
A
WT
ΔtssJ
ΔtssM
ΔtssL
sfGFP-TagL
ΔmltE
ΔtssK
ΔtssA
ΔtssBC
B
sfGFP-TssM
sfGFP-TssL
sfGFP-TssA
TssK-sfGFP
TssB-mCh
WT
ΔtagL
C
TssJ
TssM
MltE
LTG
TssA
TssL
TagL
TssEFGK-VgrG
baseplate
Hcp
TssA
TssBC
TagA
Sheath
contraction
ClpV